

Differential Orientation of 10T1/2 Mesenchymal Cells on Non-Uniform Stretch Environments

WJ Richardson*, DD van der Voort*, E Wilson[†], JE Moore Jr.^{*,‡}

Abstract: Non-uniform stress and strain fields are prevalent in many tissues *in vivo*, and often exacerbated by disease or injury. These mechanical gradients potentially play a role in contributing to pathological conditions, presenting a need for experimental tools to allow investigation of cell behavior within non-uniformly stimulated environments. Herein, we employ two *in vitro* cell-stretching devices (one previously published; one newly presented) capable of subjecting cells to cyclic, non-uniform stretches upon the surface of either a circular elastomeric membrane or a cylindrical PDMS tube. After 24 hours of cyclic stretch, 10T1/2 cells on both devices showed marked changes in long-axis orientation, with tendencies to align parallel to the direction of minimal deformation. The degree of this response varied depending on location within the stretch gradients. These results demonstrated the feasibility of conducting cell mechanobiology investigations with the two novel devices, while also highlighting the experimental capabilities of non-uniform mechanical environments for these types of studies. Such capabilities include robust data collection for developing mechanobiological dose-response curves, signal threshold identification, and potential spatial targeting for drug delivery.

1 Introduction

It is widely known that cells of many types alter their behaviors in response to mechanical stimulation. One such behavior is altered cellular orientation dependent upon the direction of substrate stretching. Numerous studies with endothelial

* Department of Biomedical Engineering, Texas A&M University, 5045 Emerging Technologies Building, 3120 TAMU, College Station, TX 77843, USA. Tel: 979-845-5532. Fax: 979-845-4450.

[†] Department of Medical Physiology, Texas A&M Health Science Center, 336 Reynolds Medical Building, College Station, TX 77843, USA. Tel: 979-845-7816. Fax: 979-862-4638.

[‡] Corresponding Author: The Bagrit and Royal Academy of Engineering Chair in Medical Device Design. Royal Society-Wolfson Research Merit Award Holder.

Department of Bioengineering, Imperial College London, South Kensington Campus, Royal School of Mines Building, Room 4.14, London, SW7 2AZ, United Kingdom. Tel: +44 (0)20 759 49795. Fax: +44 (0)20 7594 9817. Email: james.moore.jr@imperial.ac.uk

cells (ECs), fibroblasts and smooth muscle cells (SMCs) have demonstrated that, *in vitro*, cells will tend to align parallel to the direction of minimal stretch [1-6]. In true uniaxial environments, minimal stretch occurs perpendicular to the direction of loading. ‘Simple uniaxial’ setups, wherein the transverse edges are unrestricted, actually create biaxial stretch environments due to lateral compression; in such cases, the direction of minimal stretch is slightly off-axis. The degree of cellular alignment response typically correlates to the magnitude and duration of stretch imposed upon the matrix, or the relative ratio of principal stretch components in biaxial stretch cases [5, 7]. The mechanism for this orientation response is suspected to be mediated by the remodeling of the cytoskeleton via stretch-dependence of actin assembly and disassembly rate constants [8].

Understanding the orientation behavior of cells is important as alignment plays vital roles in numerous physiologic and pathologic conditions. For instance, SMCs in the artery wall are oriented primarily in the circumferential direction in a slightly helical fashion, which is important to function as it optimizes the cells’ ability to control lumen size via contraction and dilatation [9, 10]. Also, arterial EC alignment is indicative of vascular health but randomly orientated cell populations correlate to atherogenic behaviors [11]. Our ability to understand cell orientation behavior is important to understanding disease development as well as potentially controlling this behavior to improve function of engineered tissue constructs.

Linking cell orientations to their local mechanical stimuli within the body is made difficult by the complexity of *in vivo* stress and strain environments. For example, morphogenic structures have been shown to include large spatial variations in stress and strain. Taber and colleagues quantified the strain-environment of the chick head fold during embryological development revealing stark non-uniformities [12]. In computational models, these distributions have been predicted to play important roles in achieving final tissue form [13]. Similarly, Chen and colleagues have demonstrated how spatial variation in cell-generated traction forces can arise within cell populations cultured on micropatterned surfaces of various shapes, indicative of the diverse geometric forms taken by developing tissues [14].

In addition to the morphogenic environment, stretch in a mature artery wall can also be highly non-uniform, depending on location in the vasculature, presence of an atherosclerotic plaque, or implantation of a stent[15-18]. In these cases, stretch at the inner wall is much greater than stretch at the outer wall, resulting in a dramatic stretch gradient through the artery thickness. After stent implantation, there is also an introduction of stress concentrations at the ends of the implant. These stress concentrations result in gradients of stress along the longitudinal direction of the artery, with high stresses at the edge of the stent and lower stresses farther from the stent. This stark non-uniformity is presumably pathogenic and therefore,

as a result, stent designs that seek to smoothen the transition of stress from the stented region to the nearby non-stented region of the artery have been developed. In particular, the “compliance matching stent” (CMS) of Berry et al. and Rolland et al. showed improved performance over a standard non-CMS stent, with inhibited local tissue restenotic processes after implantation in swine models[19, 20]. The detailed cellular mechanisms responsible for these beneficial effects, however, remain unclear, limiting our ability to optimize similar stent designs or develop pharmaceutical regimens to prevent restenosis. Thus, there remains a need to investigate the effects of non-uniform *in vivo* loading conditions on particular cell behaviors related to disease.

Although the body’s mechanical environments are highly heterogeneous and spatially complex, the bulk history of cell stretching experiments has employed rather simple mechanical stimuli, most often uniaxial loading of cell-seeded constructs [21]. Such studies have provided important results to help develop our understanding of mechanobiological processes. Still, there remains a need to subject cells to more physiologic stretching environments, namely non-uniform stretch fields. We have previously designed and tested a cell-stretching device capable of fine-tuning stretch gradients across 2-D elastomeric membranes [22]. Herein, we describe an additional device capable of subjecting cells cultured on the outer surface of a tubular substrate to a longitudinal stretch gradient. This work analyzed the orientation responses of murine mesenchymal cells when stretched upon both devices.

2 Materials & Methods

2.1 Membrane Device Design

The device used to stretch cells cultured on elastomeric membranes has been previously described [22]. Briefly, a thin circular membrane was radially deformed in all directions via vertical displacement of its outer circumference over a stationary Teflon platen (Figure 1). The deformation was driven by a computer-controlled stepper motor (Anaheim Automation) with a rack and pinion gear connected to the clamped membrane. The motor was controlled by manufacturer-provided software (SMC50WIN) allowing precise programming of cyclic stretch amplitude and frequency. Once the device was assembled, the membrane was suspended upside-down in an enclosed Lexan box containing culture medium, and the box was kept inside an incubator at 37°C and 5% CO₂. A glass coverslip was mounted in the bottom of the box to allow imaging of the cells with an inverted fluorescent microscope (Nikon TE-2000, Nikon Instruments).

Radial deformation of a circular elastomeric membrane generates both radial and circumferential stretches. Cutting a circular defect in the center of the membrane

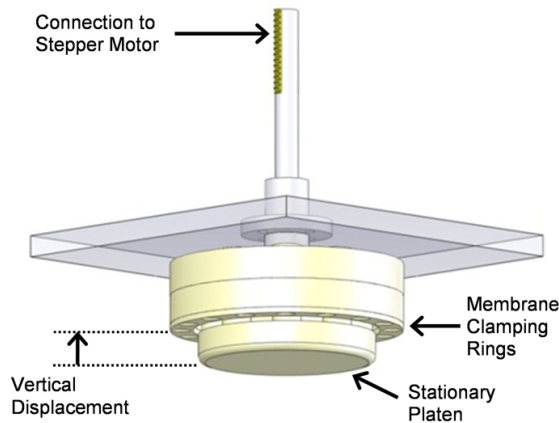


Figure 1: Membrane device schematic: A circular elastomeric membrane was radially deformed by stretching over a stationary platen driven by a computer-controlled stepper motor. Vertically displacing the clamped outer circumference of the membrane produces uniform radial loading of the membrane's edge.

produces gradients in each of these stretch components. The profiles of stretch gradients in such cases depend upon the magnitude of the displacement at the outer edge, as well as the outer and inner radii values. The solution for this finite-deformation problem has been previously solved by David and Humphrey, and the capabilities of this stretching device have been previously tested and reported [22, 23]. Importantly, with the inclusion of a central defect, circumferential stretch (λ_θ) ranged from high values at the inner edge to lower values at the outer edge, while radial stretch (λ_r) ranged from low values at the inner edge to higher values at the outer edge, but everywhere $\lambda_r < \lambda_\theta$. In this study, membranes with outer radius = 50mm and inner radius = 7.5mm were stretched with stepper-motor displacement chosen to achieve $\sim 11\%$ circumferential stretch at the inner edge.

In order to compare cellular orientation to the directions of stretch, the angle of minimal stretch was calculated for every point across the membrane. For this calculation, the equation for composite stretch, λ , was derived from the deformation gradient tensor \mathbf{F} , yielding the following:

$$\lambda^2 = \lambda_r^2 \cos^2(\phi) + \lambda_\theta^2 \sin^2(\phi) \quad (1)$$

where ϕ equals the angle measured off of the radial axis. Taking $\lambda = 1$ (minimal

perturbation of cell cytoskeleton), the angle of least stretch was calculated:

$$\phi = \arcsin \left(\sqrt{\frac{1 - \lambda_r^2}{\lambda_\theta^2 - \lambda_r^2}} \right) \quad (2)$$

Since λ_r and λ_θ varied with radial position, ϕ was a function of position as well. Also, note that Eq. 2 was only valid for $\lambda_r \leq 1$. Where $\lambda_r > 1$, of course $\phi = 0^\circ$ since $\lambda_r < \lambda_\theta$ everywhere (ie., the direction of least stretch is in the radial direction).

2.2 Tube Device Design

To subject cells to longitudinal stretch gradients on tubular constructs, a tube-stretching device was built based upon tube inflation theory used by Mohammad et al. and Rachev et al [24, 25]. Briefly, a thin elastomeric tube was implanted with an oversized, cylindrical rigid insert (Figure 2). When the tube was subsequently inflated by an intramural pressure wave, circumferential and longitudinal stretches are generated. The oversized insert introduces a boundary condition resulting in large variations of these stretch components depending on their location upon the tube.

Tubes were manufactured using Sylguard 186 (Dow Corning, MI), a silicon based polymer solution. After mixing with a curing agent (10:1 ratio of polymer: curing agent), the mixture was poured into a mold consisting of FEP shrink tubing (ID =5.25mm) mounted around a stainless steel inner mandrel (D=4.4mm). Once poured, the elastomer was cured by heating in an oven at 80°C overnight. After curing, the shrink tubing was removed, and the tube was slid off the inner mandrel using ethanol as a lubricant. Final dimensions of the cylindrical tube were 50mm in length with 5.25mm outer diameter and 4.4mm inner diameter (0.425mm thickness). For the rigid insertion, a cylindrical glass segment (10.0mm in length, 6.0mm outer diameter,) was manually inserted and positioned at the center of the tube. Post manufacturing, tubes were autoclaved in deionized water, hydrophilized by soaking in 70% sulfuric acid for 60 seconds, autoclaved again, and stored in DI water.

For inflation, tubes were cannulated and secured to metal tube attachments, and connected to a flow loop consisting of a gear pump (Ismatec BVP-Z; Ismatec SA, Switzerland) driven by a function generator (BK Precision 4016; BK Precision, CA), a glass compliance chamber, a resistance valve and a supply reservoir (Figure 2). These elements allow for a wide variety of pulsatile pressure waveforms to be generated for tube inflation. The tube and its connections were housed inside a culture chamber to hold cell-culture medium. This box also contained a glass

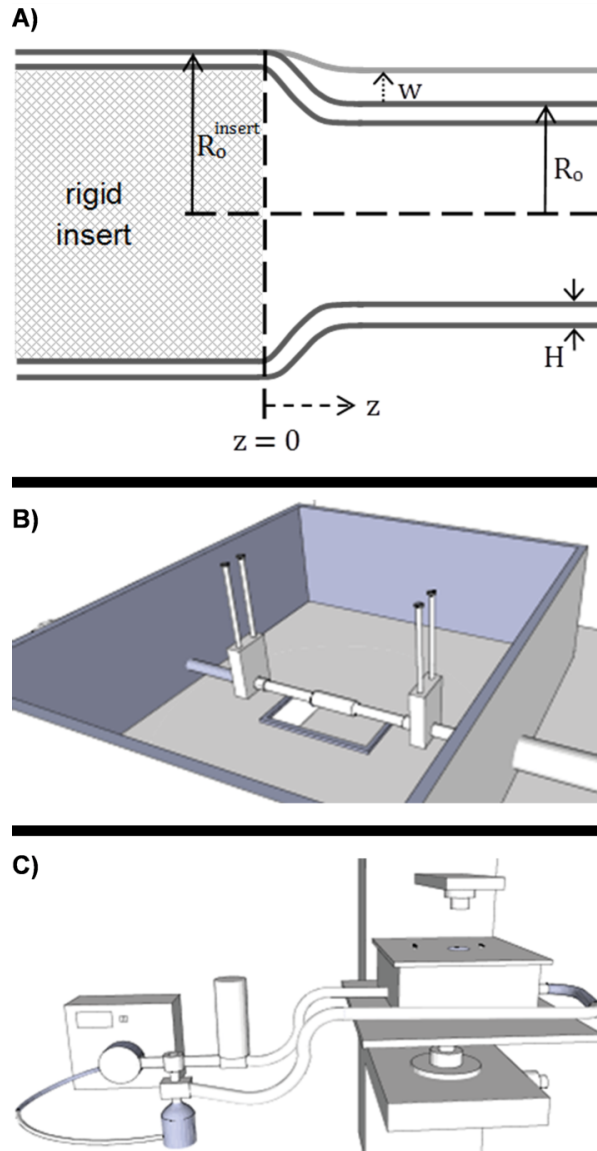


Figure 2: Tube experimental setup: Thin-shell theory was used to calculate radial wall displacement, w , as a function of the longitudinal position, z , relative to the edge of the insert (A). For experiments, a cell-seeded PDMS tube containing an oversized glass insert within a short segment of the tube was enclosed within a culture box (B) to contain cell-culture medium, with a glass coverslip in the bottom of the box to allow imaging via inverted microscopy. The connected flow loop (C) consisted of a gear pump driven by function generator, a capacitance reservoir, and a resistance valve over a supply reservoir.

coverslip on the bottom surface to allow for imaging with a Nikon TE-2000 inverted fluorescent microscope (Nikon Instruments, Japan).

2.3 Tube Device Deformation Field

As in Mohammad et al. and Rachev et al., thin-shell theory is applied to estimate deformations of a cylindrical tube stretched over a rigid insert [24, 25]. The ‘thin tube’ assumption requires the thickness:radius ratio to be negligibly small, allowing for simplification of the governing motion equation derived from equilibrium and displacement boundary conditions. By also assuming the tube is linearly elastic, isotropic ($E_\theta = E_r = E$), and incompressible ($\mu = 0.5$), the equilibrium equation for the case of tube deformation by a uniform radial pressure reduces to a 4th-order, linear ODE of radial displacement of the mid-wall surface, w (measured positive inward), as a function of longitudinal position, z . The linear elasticity assumption is justified since the end-goal is to estimate stretches, which requires only the displacements rather than the calculation of stresses, and the displacements (rather than pressures) are calibrated experimentally. For deformations caused by rigid insertion and pressurized inflation, boundary conditions were enforced for the edge behaviors in order to restrict the wall displacement at the insert to be exactly determined by the size of the insert, the wall displacement far from the insert to be exactly determined by the inflation due to intraluminal pressure change, and the wall displacement transitions to be smooth along the entire length of the tube (from $0 < z < \infty$). These restrictions result in the following solution:

$$w(z) = \frac{PR_0}{EH} + \left(\frac{R_0^{insert} - R_0}{R_0} + \frac{PR_0}{EH} \right) (\sinh(kz) - \cosh(kz)) (\sin(kz) + \cos(kz))$$

with

$$k = \sqrt{\frac{3R_0}{2H}} \tag{3}$$

This displacement, w , is the dimensionless wall displacement (normalized by R_0) from a straight, undeformed tube to a pressurized tube with a rigid insert. Given the undeformed radius of the tube, R_0 , undeformed tube thickness, H , radius of the rigid insert, intraluminal pressure, P , and linearized elastic modulus of the tube, E , the solution can be used to give the deformed tube wall position profile.

$$e_\theta = -\frac{\bar{w}}{R_0} \tag{4}$$

$$e_z = -\frac{d^2\bar{w}}{dz^2}(r^*) \tag{5}$$

where the overbar denotes actual (dimensional) values, and r^* is the radial distance of from the mid-wall surface ($r^* = -0.5 \times \text{thickness}$ for the outer wall). In our experiments, the tube was cyclically inflated from a diastolic pressure to a systolic pressure, after the rigid insert had been implanted. To calculate stretches between these two conditions, w is used to find the tube wall positions at both diastolic and systolic time points. The circumferential and longitudinal stretch values for deformation between diastolic and systolic inflation (and the respective stretch, λ) can then be calculated with the following:

$$e_{\theta,z} = \frac{e_{\theta,z}^{\text{systolic}} - e_{\theta,z}^{\text{diastolic}}}{e_{\theta,z}^{\text{diastolic}} + 1} \quad (6)$$

$$\lambda_{\theta,z} = 1 + e_{\theta,z} \quad (7)$$

The deformation analysis accurately estimates the levels of stretch as they vary from the edge of the rigid insert to the end of the tube. This variation provides an experimental region to study the effects of stretch gradients on cell behavior.

2.4 Cell Culture & Stretching

For cell stretching experiments, 10T1/2 cells (ATCC CCL-226) were cultured in SMGM with 5% fetal bovine serum, and antibiotics (Lonza). The 10T1/2 cell line is a murine mesenchymal cell, used for its relevance to a variety of fully differentiated cell types, particularly SMCs [26]. Prior to cell-seeding, the surface of circular membranes (diameter = 10mm; cut from 0.5mm thick silicone sheeting (Specialty Manufacturing Inc., MI) and outer surface of tubes (described above) were coated in bovine fibronectin (Sigma-Aldrich) by submerging for 1.5 hours in a fibronectin-PBS suspension to yield a surface area concentration of $5\mu\text{g}/\text{cm}^2$. Membranes and tubes were then washed with PBS, washed with medium, and then submerged in medium containing 10T1/2 cells (between passages 10-15) in suspension. Cell concentration in suspension was chosen to yield a seeding density of 10^4 cells/ cm^2 . Each tube was slowly rotated for several hours post seeding to enable uniform seeding around its outer surface. Both constructs were subsequently incubated for 2 days prior to stretching to ensure adequate adhesion.

After 2 days incubation, membranes were attached to the stretching device and cyclically deformed at 1Hz for 24hours according to the stretch profile described above. Tubes were stretched via cyclic inflation at 1 Hz for 24 hours, with pressurization level selected to yield 10% circumferential stretch far from the rigid insert.

2.5 Orientation Analysis

After stretching, cells were imaged with bright field microscopy at 10x magnification. Across the membrane, images were captured at ~ 50 positions using a motorized stage to collect image coordinates. Radial position of each image was calculated by estimating the membrane's center based on a circular fit of the points around the inner edge. Within each image, the orientation of every cell was calculated using ImageJ software (NIH). Cell outlines were manually traced and fit to ellipses using ImageJ's algorithm. This fit maintains the cell's total area and orientation direction. Each cell's orientation angle (measured from the horizontal axis of the image) was adjusted for the image's position on the membrane to give the angle measured off the radial direction. This angle was further adjusted for the direction of minimal stretch as a function of radial position, calculated by Eq. 2 above. The resulting angle for each cell describes that cell's angle away from the direction of minimal stretch, ranging from 0° (parallel to minimal stretch) to 90° (perpendicular to minimal stretch). Cell elongation was also calculated, quantified for each cell as the aspect ratio of the fitted ellipse.

For the tube setup, images were captured above the rigid insert, far from the rigid insert, and within the transition region. Cell alignment was again quantified using ImageJ with orientation angle defined between a cell's major axis and the longitudinal direction of the tube.

2.6 Statistical Analysis

Orientation histograms were generated for each microscope image, dividing cells into 5° orientation bins between 0° and 90° . Images were grouped ($n=2-9$) according to their position upon the membrane or tube setups and overall histograms for each position group were generated by averaging histogram values of individual images within the group. To analyze the degree of cell alignment at various positions (and therefore at various stretches), circular statistical techniques were applied. Briefly, cell orientation angles were translated into x- and y-components, which were then averaged for all cells from all images within each group. The length of the resultant mean vector is a measure of alignment that varies from 0 (perfectly random) to 1 (perfect alignment). These mean vector lengths (MVLs) were tested for statistical significance using Rayleigh's test for randomness. Linear regression analysis was used to fit the response of elongation to mechanical stimulus. Averaged data are reported as mean \pm st. deviation.

3 Results

3.1 Stretch Field Characterization

Radially deforming a circular elastomeric membrane with a central defect generated gradients in circumferential and radial stretch components (Figure 3). With the selected membrane geometry and loading regimen, circumferential stretch decreased from 1.11 at the inner edge to 1.03 at the outer edge, while radial stretch increased from 0.95 at the inner edge to 1.02 at the outer edge. These variations result in a ‘simple uniaxial’ stretch environment near the inner edge that transitions to a near equi-biaxial stretch environment at the outer edge. Stretch gradients are steep near the center and shallower further from the center. Due to the non-uniformity in the stretch components, the resultant angle of minimal stretch varies with membrane position (Figure 3), decreasing from 33.8° off the radial axis at the inner edge to 0° (parallel with the radial axis) from $r = 14.5\text{mm}$ and outward.

Tube deformation profiles were calculated using the governing displacement equation (Eq. 3) and the stretch relations (Eq. 7) for potential stretching cases yielding far-field circumferential strains of either 10% or 20% (Figure 4). Above the rigid insert ($z \leq 0\text{mm}$), the tube wall does not move with inflation. Far from the glass insert ($z \geq 3\text{mm}$), the tube wall displacement is nearly uniform, and solely dependent upon the intraluminal pressure increase. When the tube is inflated from the baseline (diastolic) to either the 10% or 20% case (systolic), there is no stretch above the glass insert and strip-biaxial stretch ($\lambda_\theta > 1$, $\lambda_z = 1$) far from the glass insert, with a highly non-uniform biaxial stretch transition in between. For the nominal 10% case, circumferential stretch varies from 1.0 at the glass edge to 1.10 far field, while longitudinal stretch varies from 0.91 at the glass edge to 1.0 far field. Notably the longitudinal stretch profile peaks at nearly 1.04 before falling back to 1.0. This biphasic behavior arises from the bending-inflation interactions within the transition zone. For the 20% case, the trends are identical with circumferential stretch varying from 1.0 to 1.20, and longitudinal stretch varying from 0.82 to 1.0 with a peak at 1.07.

3.2 Cellular Orientation Response

Prior to stretching, 10T1/2 cells seeded on both the membrane and outer surface of the tube showed good viability and adequate adhesion to the substrate. After 24 hours of cyclic stretch, cells remained adhered to both surfaces with healthy morphology and obvious orientation changes (Figures 5-7). These changes demonstrated a tendency for cells to orient parallel to the local direction of least stretch. On the membrane, the degree of this response varied greatly correlating to radial position (Figures 5, 7). High alignment tendencies were evident among cells sub-

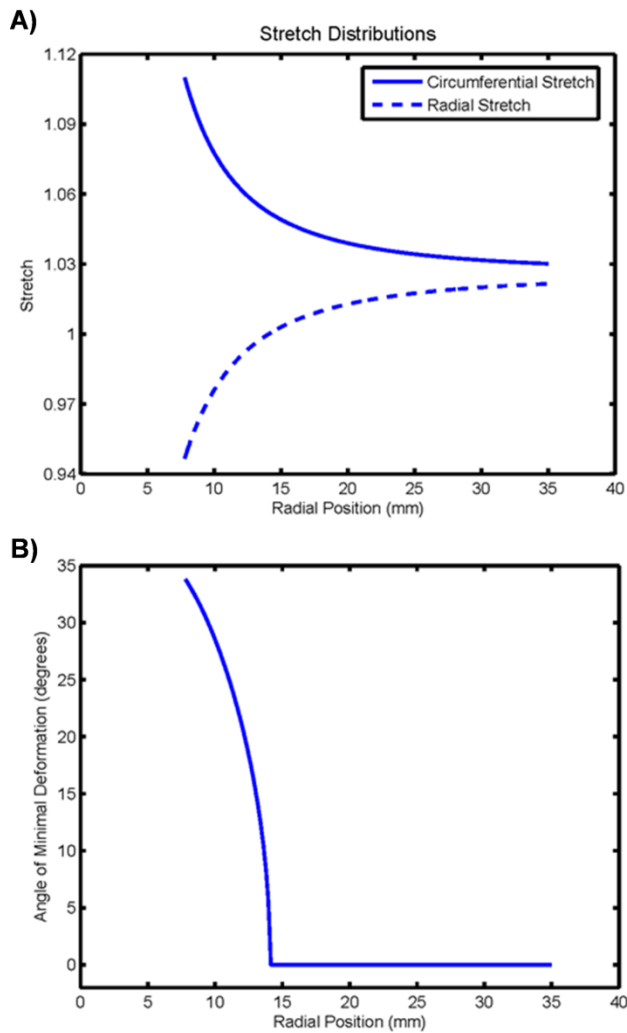


Figure 3: Membrane stretch profile characterization: Radially deforming a circular membrane with a central defect generated gradients in both circumferential and radial stretch components (A). The off-axis direction of minimal stretch varied with radial position due to circumferential: radial stretch ratio variation (B).

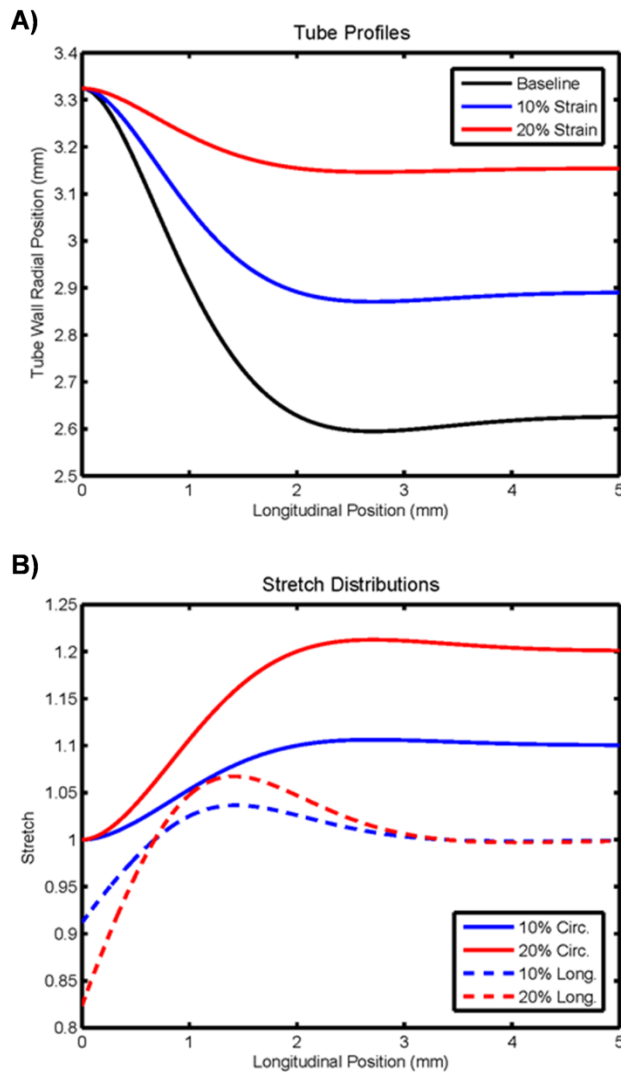


Figure 4: Tube geometries and stretches: A thin-walled tube was implanted with a rigid cylindrical insert and subsequently subjected to cyclic inflation. The tube geometric profile (A) and stretches (B) were calculated for cases of 10% and 20% nominal stretch, defined by the circumferential stretch far from the rigid insert between systolic and diastolic configurations.

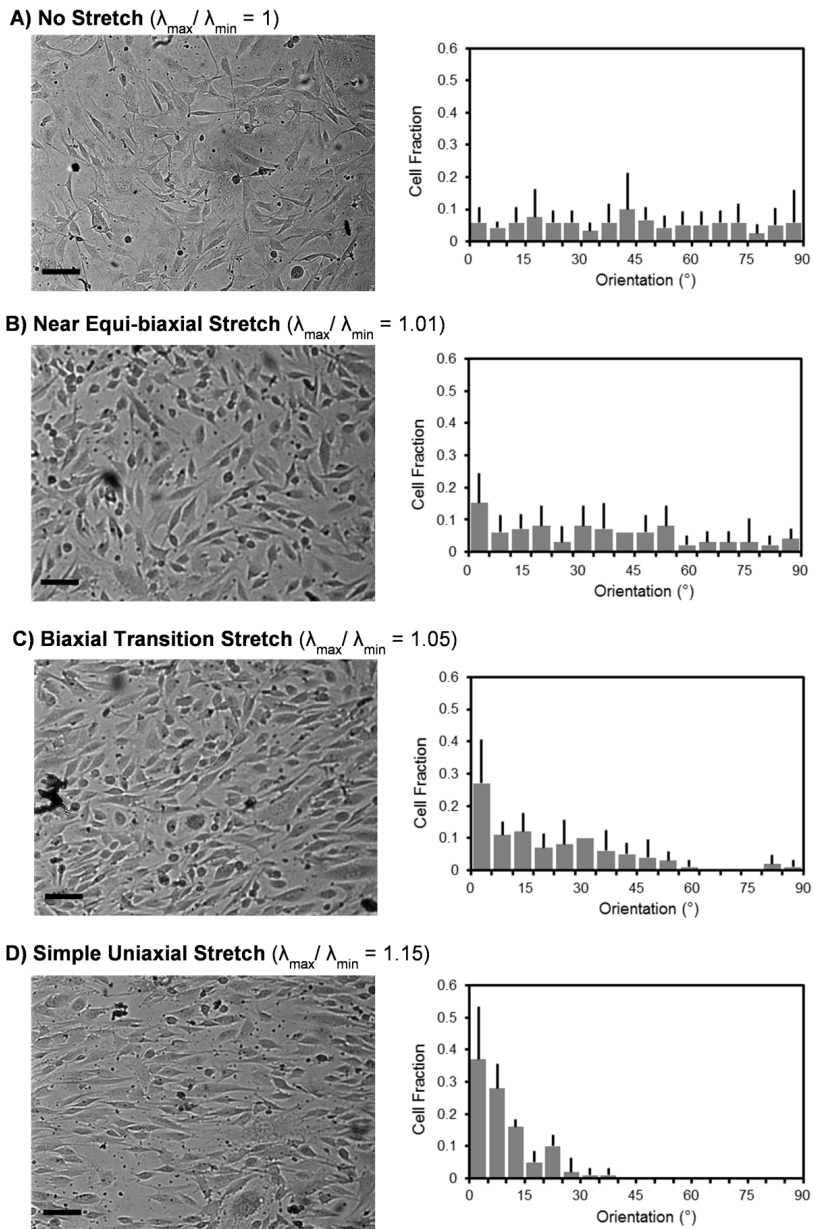


Figure 5: 10T1/2 cell orientation on membranes: Before stretch, 10T1/2 cells oriented randomly on elastomeric membranes (A). After 24hrs of cyclic stretch, cell alignment varied with radial position, from random alignment under near equibiaxial stretch (B) to high alignment under simple uniaxial stretch (D). Scale bars equal 100 microns.

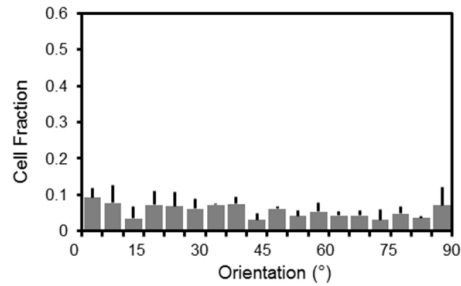
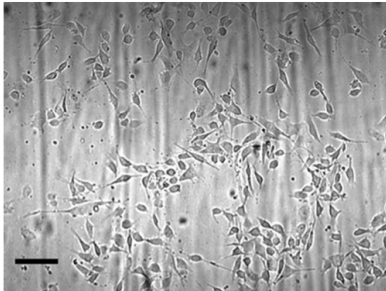
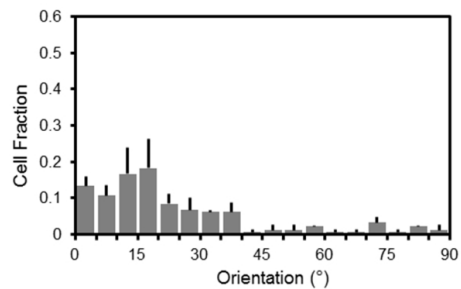
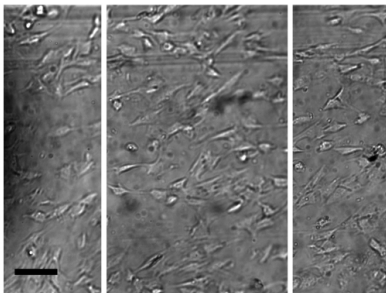
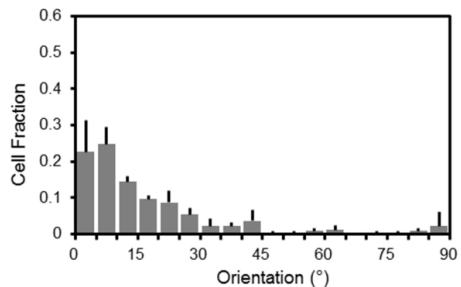
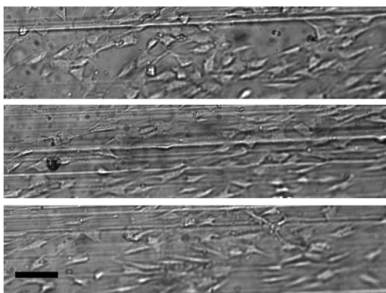
A) No Stretch ($\lambda_{\max}/\lambda_{\min} = 1$)**B) Biaxial Transition Stretch** ($\lambda_{\max}/\lambda_{\min} = 1.06$)**C) Strip Biaxial Stretch** ($\lambda_{\max}/\lambda_{\min} = 1.10$)

Figure 6: 10T1/2 cell orientation on tubes: After 24 hours of cyclic stretch, the orientation of 10T1/2 cells on the outer surface of PDMS tube constructs varied with longitudinal position. Above the rigid insert, cells demonstrated no particular alignment (A). Within the transition zone of biaxial stretch, cells demonstrated moderate alignment in the longitudinal direction (B). Far from the glass insert, cells demonstrated strong alignment in the longitudinal direction, which corresponds to the direction of minimal deformation (C). Scale bars equal 100 micrometers.

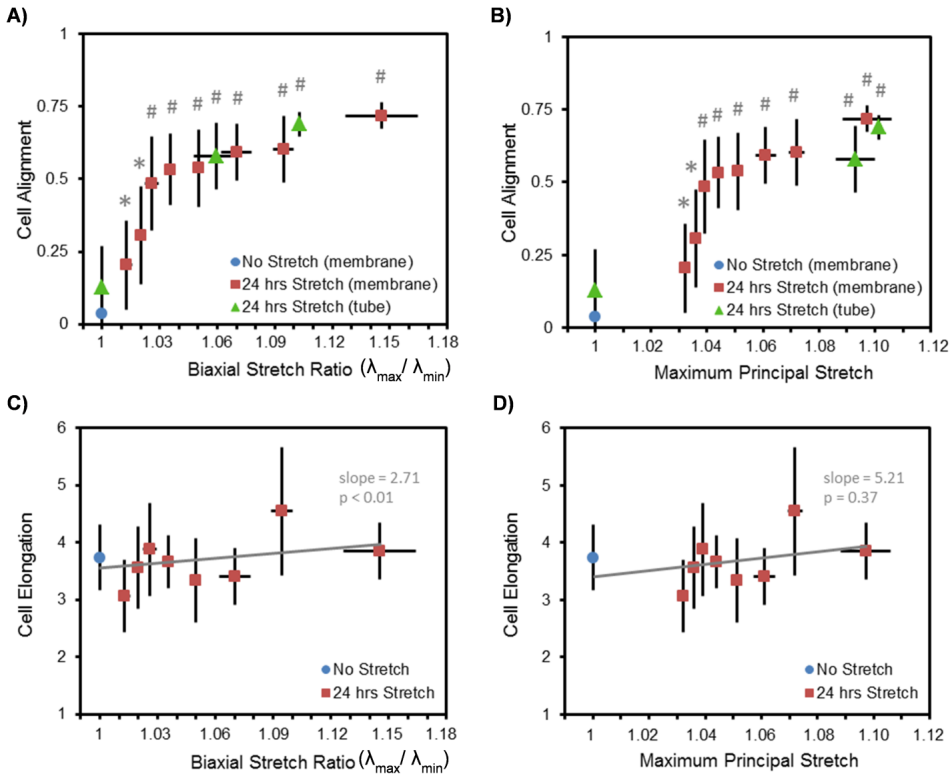


Figure 7: 10T1/2 cell alignment metrics: Cell alignment (quantified as the length of grouped cells' mean orientation vector) varied strongly with biaxial stretch ratio on both the membrane and tube setups (A). Cells exhibited very low alignment under no stretch or near equibiaxial stretch, and very high alignment under uniaxial stretch. Rayleigh's test for randomness revealed statistically significant alignment at $p < 0.01$ (*) or $p < 0.001$ (#). Cell alignment also varied with maximum principal stretch component but did so less smoothly (B). Cell elongation (quantified as the aspect ratio of an ellipse fit to each cell's outline) varied very slightly with biaxial stretch ratio (C) and maximum stretch component (D), according to linear regression analyses.

jected to uniaxial stretch near the center, while lower alignment tendencies were seen among cells in near equibiaxial stretch far from the center. A smooth transition of alignment occurs along the radial positions between the two extremes.

On the tube device, the degree of alignment varied with longitudinal position (Figures 6-7). Cells located above the rigid insert were subjected to no stretch and showed no alignment tendencies, while cells located far from the insert were subjected to strip biaxial stretch ($\lambda_\theta > \lambda_z = 1$) and showed a strong tendency to align longitudinally. Within the transition region of biaxial stretch, there is a smaller tendency for longitudinal orientation.

A dose-response behavior of cell alignment as a function of mechanical stimuli across both the membrane and tube constructs was clearly exhibited by the increasing relationship of cellular mean vector length versus the local ratio of maximum stretch component to minimal stretch component (Figure 7A). Interestingly, the curve exhibits a clear inflection point at a stretch ratio around 1.03 corresponding to a MVL around 0.5. Before this point, cell MVL quickly rises with stretch ratio increasing from 1.0 (corresponding to no stretch or perfect equibiaxial stretch); but after this point, further increases in stretch ratio produce smaller increases in cell MVL. Also interestingly, the relationship between cell MVL and the local maximum stretch component (λ_θ) was not as smooth as that with the biaxial stretch ratio (Figure 7B). The increases in cell alignment were not coincident with much change in cell elongation measurements, which showed a trend to increase only very slightly with increasing biaxial stretch ratio or maximum stretch component (Figure 7C and 7D, respectively)

4 Discussion

There is a pressing need for *in vitro* studies to subject cells to the realistic, spatially varying mechanical environments imposed in health and disease. Herein, we have demonstrated the feasibility of two cell-stretching devices designed to investigate cellular responses to non-uniform strain fields. By radially deforming a circular elastomeric membrane with a central defect, we can generate controllable gradients in radial and circumferential stretch components. Additionally, by inserting an over-sized rigid fixation into an elastomeric tube and subsequently inflating the tube, we can create a longitudinal gradient in circumferential and longitudinal stretch components. 10T1/2 cells subjected to these stretching environments for 24 hours changed their alignment depending upon their location within the stretch gradients. As anticipated, cells adhered to regions of highest stretch demonstrated strong alignment tendency parallel to the direction of minimal stretch, while cells adhered to regions of low stretch or near equi-biaxial stretch demonstrated more random orientations. This behavior is consistent with numerous previous investiga-

tions that indicate cells of many types align in the direction of minimal deformation [1-6].

The vast majority of previous cell stretching devices subjected cultures to simplified mechanical stimuli. Several recent devices, however, have sought to represent more physiologic-like environments by incorporating non-uniform strain fields into culture substrates. For example, Ohashi et al created a spatial gradient in strain by uniaxially loading a rectangular elastomeric membrane with a circular glass disc embedded in the center [27]. ECs stretched with this device demonstrated marked changes in stress fiber organization depending on location along the gradient. In similar fashion, Yung et al generated strain gradients by uniaxially loading PDMS wells with rectangular glass strips bonded to the bottom surface [28]. The non-uniform strain profile on this device was characterized but cell behaviors at different points along the gradient were not analyzed.

Balestrini et al extended the rigid-fixation strategy to biaxial loading environments by employing the commercially available Flexcell system to stretch 2D membranes and 3D fibrin gels with a glass disc secured as a central fixation [7]. This setup generated radial gradients in both circumferential and radial stretch components, similar to the environment created by our device but with opposite relative magnitudes of the stretch components (ie., radial stretch was greater than circumferential stretch in their setup). When loaded with their device for several days, dermal fibroblasts showed varied alignment tendencies across different positions upon the membrane. With an alternative approach, Tan et al used topographical patterns (circumferential or radial grooves) to create nonuniform anisotropy in strain upon circular membranes [29]. They found differential patterns of vascular SMC proliferation and nuclear shape across these gradients. However, their experiments restricted cell orientation to align with the imposed microgrooves regardless of local stretch components, thereby limiting their ability to elucidate cell behavior when stretched on a 'free' surface without contact guidance cues. This recent handful of studies has revealed the great potential of non-uniform stretch environments within mechanobiological investigation for linking cell behavior to many levels of mechanical loading with single experiments. This capability is useful for efficiently collecting more complete data sets to build and test theoretical models of mechanobiological processes (e.g., alignment models such as those presented by Kaunas and Hsu, and De et al.) [8, 30].

With similar motivation, we have recently published a novel device employing platen displacement of a circular membrane with a central defect [22]. A unique feature of this design is that it generates a region of compressive radial strain in concert with a tensile circumferential strain. This combination is noteworthy as it represents what is seen in the *in vivo* arterial wall. Moreover, our device in fact

generates three types of stretching environments including simple uniaxial ($\lambda_{e1} > 1$, $\lambda_{e2} < 1$), strip biaxial ($\lambda_{e1} > 1$, $\lambda_{e2} = 1$), and nearly equibiaxial ($\lambda_{e1} = \lambda_{e2}$). This allows the investigation of cellular behavior in diverse environments with individual experiments. The two devices used herein reflect a move toward creating environments that attempt to directly mimic mechanical stimuli from particular implanted devices, in this case, a stented artery.

Admittedly, SMC alignment is not necessarily of greatest interest to the clinical problem of restenosis. Still, our findings demonstrate the devices' capability to successfully elicit differential cellular responses along a non-uniform stretch gradient. Since data collection and analysis for cell orientation is relatively straight-forward, we can quickly demonstrate feasibility of experimental protocols, confirm cell sensation of mechanical stimuli, and prove adequate cell viability. In addition, cellular alignment is a significant process in many other tissue behaviors, normal and diseased, such as morphogenesis wherein strain environments are highly non-uniform and potentially provide directional cues for tissue differentiation and development [14]. Our results provide a more detailed description of the dose-response behavior of 10T1/2 cell alignment as a function of biaxial stretch ratio, and suggest several interesting behaviors including the potential existence of a threshold in cell alignment and/or stretch stimulus that slows the rise of cell MVL with increasing stretch signal, and also the existence of cell alignment increases without strong concurrent increases in cell elongation.

A principal limitation of this work is the use of 2D cell culture. Many studies have revealed differences in cell behavior when cultured on 2D vs 3D substrates [31]. Still, we believe 2D cell culture is a useful first step toward creating more physiologic mechanical environments, and both devices presented can be adapted to load 3D constructs in the same fashions. An additional limitation of this work is the ambiguity of primary vs interaction effects between stretch magnitude, biaxial stretch ratio, and stretch gradients. All three of these mechanical parameters varied with spatial position upon our devices. Experiments remain to be conducted that test each of these parameters independently in order to isolate the effects of each on biological responses of interest.

Future studies with these devices will focus on cell behaviors more closely related to arterial disease formation such as SMC migration, proliferation and phenotype modulation. 3D constructs will also be incorporated to subject cells to a mechanical environment even more representative of the physiologic conditions, thereby providing additional detail and investigative capability. A particular mechanical cue that remains to be adequately investigated is a gradient in stretch and its ability to act as a directional cue for cell behavior. Although one study noted cells' ability to potentially sense directionality via strain gradients, this data was qualita-

tive and limited [27]. It would be interesting to know if stretch gradients are able to guide cell migration or division in a mechanism similar to durotactic motility. The nonuniform strain fields imposed by stenting and other conditions potentially play important roles in the development of disease as well as the success of possible treatment options. To that end, experimental devices recreating the mechanical stimuli as closely as possible can be used to help illuminate the cellular mechanisms involved in these conditions, a key step in designing adequate therapies and technologies to treat or prevent disease.

Acknowledgments

The authors gratefully acknowledge Dr. Daisuke Mori and Dr. Michael Moreno for assistance during device conception and construction, and Mr. Sean Brocklehurst for assistance with image analysis and cell culture. JEM Jr. also acknowledges the support of the Lohman Professorship at Texas A&M University, the Bagrit Trust, the Royal Academy of Engineering and the Royal Society-Wolfson Research Merit Award.

We also wish to acknowledge the current affiliation for JEM:

Department of Bioengineering, Imperial College London, South Kensington Campus, London, SW7 2AZ, United Kingdom.

Tel: +44 (0)20 7594 9795

Fax: +44 (0)20 7594 9817

and the current affiliation for WJR:

Department of Biomedical Engineering, University of Virginia, Box 800759, Health System, Charlottesville, VA 22908, USA.

Tel: 434-982-5929

Fax: 434-982-3870

References

1. Buck, R.-C. (1980) *Exp Cell Res* 127(2), 470-474.
2. Mudera, V.-C., Pleass, R., Eastwood, M., Tarnuzzer, R., Schultz, G., Khaw, P., McGrouther, D.-A., & Brown, R.-A. (2000) *Cell Motil Cytoskeleton* 45(1), 1-9.
3. Dartsch, P.-C., Hammerle, H., & Betz, E. (1986) *Acta Anat (Basel)* 125(2), 108-113.
4. Kanda, K., Matsuda, T., & Oka, T. (1992) *ASAIO J* 38(3), M382-385.

5. Kanda, K. & Matsuda, T. (1993) *Cell Transplant* 2(6), 475-484.
6. Houtchens, G.-R., Foster, M.-D., Desai, T.-A., Morgan, E.-F., & Wong, J.-Y. (2008) *J Biomech* 41(4), 762-769.
7. Balestrini, J.-L., Skorinko, J.-K., Hera, A., Gaudette, G.-R., & Billiar, K.-L. (2010) *Biomech Model Mechanobiol* 9(3), 329-344.
8. Kaunas, R. & Hsu, H.-J. (2009) *J Theor Biol* 257(2), 320-330.
9. Williams, B. (1998) *J Hypertens* 16(12 Pt 2), 1921-1929.
10. Wolinsky, H. & Glagov, S. (1967) *Circ Res* 20(1), 99-111.
11. Nerem, R.-M., Levesque, M.-J., & Cornhill, J.-F. (1981) *J Biomech Eng* 103(3), 172-176.
12. Filas, B.-A., Varner, V.-D., Voronov, D.-A., & Taber, L.-A. (2011) *J Vis Exp* (56), e3129.
13. Varner, V.-D., Voronov, D.-A., & Taber, L.-A. (2010) *Development* 137(22), 3801-3811.
14. Nelson, C.-M., Jean, R.-P., Tan, J.-L., Liu, W.-F., Sniadecki, N.-J., Spector, A.-A., & Chen, C.-S. (2005) *Proc Natl Acad Sci U S A* 102(33), 11594-11599.
15. Lally, C., Dolan, F., & Prendergast, P.-J. (2005) *J Biomech* 38(8), 1574-1581.
16. Bedoya, J., Meyer, C.-A., Timmins, L.-H., Moreno, M.-R., & Moore, J.-E. (2006) *J Biomech Eng* 128(5), 757-765.
17. Delfino, A., Stergiopoulos, N., Moore, J.-E., Jr., & Meister, J.-J. (1997) *J Biomech* 30(8), 777-786.
18. Li, Z.-Y., Tang, T., J, U. K.-I., Graves, M., Sutcliffe, M., & Gillard, J.-H. (2008) *Circ J* 72(7), 1092-1099.
19. Rolland, P.-H., Mekkaoui, C., Vidal, V., Berry, J.-L., Moore, J.-E., Moreno, M., Amabile, P., & Bartoli, J.-M. (2004) *Eur J Vasc Endovasc Surg* 28(4), 431-438.
20. Berry, J.-L., Manoach, E., Mekkaoui, C., Rolland, P.-H., Moore, J.-E., Jr., & Rachev, A. (2002) *J Vasc Interv Radiol* 13(1), 97-105.
21. Brown, T.-D. (2000) *J Biomech* 33(1), 3-14.

22. Richardson, W.-J., Metz, R.-P., Moreno, M.-R., Wilson, E., & Moore, J.-E., Jr. (2011) *J Biomech Eng* 133(10),101008.
23. David, G. & Humphrey, J.-D. (2004) *J Biomech* 37(8), 1197-1203.
24. Mohammad, Z., Moore, J.-E., Jr., Rachev, A., Berry, J.-L., & Manoach, E. (2000) *Int J Cardio Med Science* 3(1), 1-7.
25. Rachev, A., Manoach, E., Berry, J., & Moore, J.-E., Jr. (2000) *J Theor Biol* 206(3), 429-443.
26. Hirschi, K.-K., Lai, L., Belaguli, N.-S., Dean, D.-A., Schwartz, R.-J., & Zimmer, W.-E. (2002) *J Biol Chem* 277(8), 6287-6295.
27. Ohashi, T., Masuda, M., Matsumoto, T., & Sato, M. (2007) *Clin Hemorheol Microcirc* 37(1-2), 37-46.
28. Yung, Y.-C., Vandeburgh, H., & Mooney, D.-J. (2009) *J Biomech* 42(2), 178-182.
29. Tan, W., Scott, D., Belchenko, D., Qi, H.-J., & Xiao, L.(2008) *Biomed Microdevices* 10(6), 869-882.
30. De, R., Zemel, A., & Safrani, S.-A. (2007) *Nature Physics* 3, 655-659.
31. Pedersen, J.-A. & Swartz, M.-A. (2005) *Ann Biomed Eng* 33(11), 1469-1490.

